Ion Impingement Limits of Sub-Scale Ion Optics: Comparison of Simulation and Experiment

Joseph Wang*, Yong Cao†, and Raed Kafafy†
Virginia Polytechnic Institute and State University, Blacksburg, VA 24061-0203
Rafael Martinez‡, and John Williams§
Colorado State University, Fort Collins, CO 80523

Experiments and simulations are carried out to investigate direct impingement on accel grid using sub-scale ion optics. Good agreement is observed between measurements and simulations of the cross-over limit. When the effects from charge-exchange current and leakage current are taken into account, modeling reproduces almost exactly the measured impingement current behavior.

I. Introduction

The behavior of the accelerator grid current defines the operational envelope of an ion optics system. Under normal operating conditions, the ions in the discharge plasma upstream of the screen grid should form focused ion beamlets when extracted and accelerated through the optics. However, if the discharge plasma density is too low, the ion beamlet may become over-focused by the upstream sheath, resulting in cross-over ion impingement on the acceleration grid. On the other hand, if the discharge plasma density is too high, the ion beamlet may become under-focused, resulting in direct interception of beam ions by the acceleration grid (perveance limit). Thruster operation that results in direct impingement will cause excessive sputter erosion of the accelerator grid. Some of the sputtered material will build up into thick films on the screen grid, and one ion thruster failure mode involves shedding of these sputter deposited films. Accurate predictions of the cross-over limit and the perveance limit are needed to ensure long-term, trouble-free operation.

Most existing ion optics models are either axi-symmetric models or three-dimensional models constructed for a cross section of one twelfth of a single aperture (a 30 degree by 60 degree right-triangle cross section) using the six-fold hexagonal symmetry of the aperture array. Because of the inherent symmetric boundary conditions, existing models are suitable for local simulations of a single ion beamlet for an aperture located near the center of the optics grid. Existing modelling predictions of important ion optics parameters, such as the cross-over limit, perveance limit, and backstreaming limit, are all based on extrapolations of single beamlet simulations, where one uses different upstream plasma conditions to represent apertures at different locations on the grid surface. Previously, numerical simulations based on a single aperture model were carried to model the impingement limit for the Carbon Based Ion Optics (CBIO) gridlet.[1] While the simulation gave good predictions of the perveance and backstreaming limits, it did not indicate a crossover limit for much of the operating voltage range for the CBIO geometry.[2,3] Both the disagreement between simulation and experiment and the results from ongoing experimental studies at Colorado State University (CSU) suggest that the effects of geometric asymmetry and plasma sheath interaction between adjacent holes, may have a significant influence on the cross-over limit. Such effects could explain why early numerical modeling programs in the electric propulsion community typically predict a crossover limit value that can be 50% lower than the experimentally measured value.

A new optics model was developed recently at Virginia Tech (VT) for three-dimensional global simulations of plasma flow in an entire sub-scale ion optics.[4] This model explicitly includes apertures located near the

*Associate Professor, Department of Aerospace and Ocean Engineering, AIAA Associate Fellow. jowangvt.edu
†Postdoctoral Fellow, Department of Aerospace and Ocean Engineering
‡Graduate Research Assistant, Department of Mechanical Engineering
§Assistant Professor, Department of Mechanical Engineering

edge of the grid surface and fully accounts for the effects of multiple ion beamlets and geometric asymmetry. Simulations using this new model were carried out for a 7-aperture optics gridlet and the results were compared with that from a single-aperture model. It was shown that while a single aperture model is adequate for modelling an aperture located in the center of the optics grid, it cannot resolve the quantitative differences in plasma sheath and beamlet behavior between the center aperture and the circumferential apertures.[4]

This paper presents an experimental and simulation study to understand the accel grid impingement current for a sub-scale set of high specific impulse ion optics. The emphasis is on the comparison of the predictions of the cross-over limit by the new ion optics model described in Ref. 4 with experimental data. Section II discusses the sub-scale ion optics gridlet used for this study, experimental procedure, and experimental results. Section III discusses the simulation model, simulation result, and comparison between simulations and measurements. Section IV contains a summary and conclusions.

II. Experimental Study

A. Subscale Gridlets

Sub-scale ion optics gridlets are often used to investigate the behavior of full-sized optics in experimental studies. The sub-scale ion optics investigated here has a geometry identical to the grids developed for CBIO.[1] The objective of the CBIO program was to develop carbon grids for the NASA Evolutionary Xenon Thruster (NEXT) that will operate at a nominal Isp of 4000 sec. The CBIO program successfully completed a 1000 hr wear test of 30-cm carbon-carbon ion optics in addition to meeting performance requirements, validating grid life models, low recycle rates, and vibration testing.[5] Perveance, crossover, and electron backstreaming data are documented over wide throttling ranges.

Figure 1 shows a photograph of the various screen gridlets tested in this study, each with a different number of apertures. Table 1 shows the ion optics geometrical parameters. The discussions in this paper will focus on the 7-aperture gridlet. Table 2 lists some of the operating conditions considered in the study.

Table 1. Dimensions of the sub-scale ion optics used in this study

screen hole diameter, d_s	2.305 mm
screen grid thickness, t_s	0.461 mm
acceleration hole diameter, d_a	1.396 mm
acceleration grid thickness, t_a	1.016 mm
screen to acceleration grid gap, l_g	0.810 mm
center-to-center hole spacing, l_{cc}	2.674 mm)

Table 2. Throttling condition of the ion optics.

net acceleration V_N	screen grid voltage V_s	accel grid voltage V_a
800V	770V	-140V
1000 V	970V	-150 V
1200 V	1170V	-166 V
1420 V	1390V	-170 V
1600 V	1570V	-176 V

B. Apparatus and Procedures

Experimental studies of the sub-scale gridlet were performed at CSU. The gridlet test facility (shown in Figure 2 with the ion source installed) has a volume of $0.65m^3$ and a base pressure in the mid 10^{-7} Torr range. When the ion source is running at typical xenon flow rates, the pressure is 1×10^{-5} Torr. The facility is equipped with a cryopump to eliminate the concern that an oil-based system would interfere with the

experiments. The gridlets are placed at about 70cm away from a graphite target attached to the top of the chamber. Quartz heaters were installed that allow for bake out of the chamber. The chamber is also well equipped for future diagnostic work with 53 feed throughs that are available on the chamber floor, 7 around the sides, and 6 at the top.

Tests were conducted by mounting an assembly comprised of two gridlet electrodes to a ring-cusp discharge chamber. The grids were fabricated from Poco graphite using a computer controlled milling center. The screen and accelerator gridlets were insulated from one another using standoff insulators and were aligned through the use of precision-placed alignment holes. The inner diameter of the discharge chamber was much larger than the active diameter of the gridlets to ensure that the discharge chamber plasma properties would be uniform over the entire gridlet area, and thereby impose common behavior in all beamlets. The uniform discharge plasma condition allowed division of the measured beam current (J_B) by the number of apertures to obtain the per hole or beamlet current (J_b). A ground screen was placed between most of the inactive area of the accelerator grid and the beam plasma to limit the collection of beam plasma ions on the inactive regions of the accelerator gridlet surface. The impingement current collected by the accelerator grid (J_A) was converted to a per beamlet value (J_a) by dividing the ammeter reading by the number of active accelerator grid apertures. Typical impingement data are displayed by plotting the ratio of J_a/J_b versus J_b. Limits on the beamlet current occur at both low and high values where processes occur that drive energetic beam ions directly into the accelerator grid.

C. Experimental Results

Figure 3 contains accel grid impingement current data over a wide range of net voltages for the 7-aperture gridlet. The data are for the nominal accel and screen grids at a grid gap of 0.81 mm. Only a few of the impingement curves recorded are shown for clarity purposes. Typical accel grid impingement current data display a "U" shape when plotted as a ratio of impingement-to-beamlet current versus beamlet current.

In this experiment, the beamlet current was varied by varying the discharge current while holding the discharge, beam, and accel voltages constant. At low beamlet currents, the relative impingement current rises due to crossover ion impingement on the downstream edge of the accel hole barrels. At moderate beamlet currents, the relative impingement current is flat and at a value dependent upon the background neutral density and the propellant utilization efficiency of the ion source. In our small vacuum facility operating at low propellant utilization, the relative impingement current typically lies between 1% and 6% of the beam current. The background gas increases the amount of charge-exchange collisions, resulting in higher currents to the accelerator grid. As the beamlet current is increased to higher values, the relative impingement current will again rise quickly indicating that direct ion interception is occurring on the upstream edge of the accel hole barrels due to perveance (or space-charge) limitations.

Figure 4 shows the impingement current for 7-aperture gridlet at net accelerating voltage $V_N = 1600$V as well as the quantitative parameter used to define the cross-over and preveance limit from experimental data. The measured accel current J_a include not only the contribution from direct ion impingement J_{imp}, but also that from the collection of the charge exchange ions J_{cex} and the leakage current in the system $J_{leakage}$

$$J_a = J_{imp} + J_{cex} + J_{leakage} \tag{1}$$

Because of the contributions from J_{cex} and $J_{leakage}$, and because of the signal to noise ratio in measurement, it is not feasible to determine the exact beamlet current at which value J_{imp} first becomes larger than zero. Hence, the cross-over and preveance limit are defined as when $J_{imp}/J_b \simeq 5.5\%$ on the experimental curve. The cross-over limit taken from these data sets are plotted in Figure 5 as a function of the total accelerating voltage.

III. Simulation Study

A. Simulation Model

The simulations are carried using a new 3-D ion optics simulation code developed at Virginia Tech.[4] This model explicitly includes apertures located near the edge of the grid surface and fully accounts for the effects of multiple ion beamlets and geometric asymmetry.

The ion optics model is based on a newly developed algorithm, the Hybrid-Grid Immersed-Finite-Element Particle-in-Cell (HG-IFE-PIC) algorithm.[6] HG-IFE-PIC is an extension of the IFE-PIC algorithm.[7,8] The

IFE-PIC algorithm is a hybrid immersed-finite-element finite-difference particle-in-cell algorithm. A major attraction of the IFE method is that it allows the use of a structured mesh generated independent of the internal object boundary to solve problems involving complex internal boundaries while retaining the accuracy of unstructured body-fit mesh based field solvers. In HG-IFE-PIC, we further allow the IFE and the PIC mesh nodes to be displaced from each other instead of being collocated. We keep the uniform Cartesian mesh for PIC but stretch the primary IFE mesh according to the local potential and plasma gradients. This allows us to use fewer elements and mesh nodes to solve the same field problem using IFE. The details of HG-IFE-PIC are discussed in Ref. 6. It was shown that this algorithm is capable of achieving the same accuracy as an unstructured body-fit mesh based PIC but with a faster computational speed. In Ref. 4, a whole ion optics gridlet model is developed using HG-IFE-PIC and a streamline approximation for beam ion flow. The accuracy of the algorithm and the simulation model is also discussed in detail in Ref. 4, 6

B. Simulation Setup

The simulation setup is shown in Figure 6. The simulation domain is a three dimensional rectangle domain which includes a quarter of the gridlet. This setup accounts for the geometric effects from a hexagonal layout of surrounded and circumferential apertures, and allows symmetric boundary conditions to be applied on planes of symmetry of the domain. In the beam flow direction, the upstream domain boundary is immersed in the discharge chamber plasma. We make no assumption about the upstream plasma sheath surface. The ion extraction is determined self-consistently from the acceleration voltage drop and the upstream plasma boundary conditions. The downstream domain boundary is placed in the neutralized propellant plasma. The last few cells next to the downstream boundary are considered as a quasi-neutral zone where the propellant ions are neutralized.[9] We take the downstream plasma density to be the average ion density within the quasi-neutral zone. Hence, the downstream plasma density is updated each time step.

Macro-particles representing the propellant beam ion streamlines are introduced into the simulation domain from the upstream boundary at each PIC time step. Each streamline is determined from the integration of its equation of motion given by Newton's second law as

$$\frac{d}{dt}(m\mathbf{v}) = \mathbf{F} = q\mathbf{E} \,, \tag{2}$$

$$\mathbf{v} = \frac{d\mathbf{x}}{dt} \,. \tag{3}$$

The electron density is considered to follow the Boltzmann distribution in the regions where electrons exist, i.e. the upstream and downstream regions of the ion optics. Specifically, in the upstream region, the electron density is given by

$$n_e = n_{e0} \exp\left(\frac{e(\Phi - \Phi_0)}{kT_{e0}}\right), \tag{4}$$

where Φ_0, n_{e0}, and T_{e0} are, respectively, the potential, electron density and electron temperature of the discharge plasma. The downstream electron density is given by

$$n_e = n_{e\infty} \exp\left(\frac{e(\Phi - \Phi_\infty)}{kT_{e\infty}}\right), \tag{5}$$

where Φ_∞, $n_{e\infty}$, and $T_{e\infty}$ are, respectively, the potential, electron density and electron temperature of the downstream neutralized plasma. The electrostatic field is solved self-consistently with the boundary condition and the space charge of the particles from the Poisson's equation

$$\nabla \cdot (\epsilon_0 \nabla \Phi) = e(n_e - n_i) \,. \tag{6}$$

As the focus of this study is to simulate the behavior of the acceleration grid impingement current and identify the cross-over limit, simulations presented here only concern the flow of the propellant beam ions. Charge-exchange ions generated between the beam ions and neutrals are not included in order to speed up the simulation. Charge-exchange ions have very little effect on the ion optics electric field and the beam ions trajectories because of their negligible contribution to the overall space charge. The inclusion of charge-exchange ions in the simulation will only change the magnitude of the impingement current slightly and is not expected to affect the cross-over limit.

To calculate the beam ion extraction properly, the upstream boundary needs to be set far enough from the screen grid and the cell size should resolve the Debye length of the upstream discharge plasma,[9] λ_{D0}. As the beam ion density decreases rapidly in the downstream region of the acceleration grid, we allow the IFE mesh to stretch gradually in the downstream region. The stretched IFE mesh is such that $\Delta z_{min} \leq lambda_{D0}$ and $\Delta z_{max} < \lambda_{D\infty}$, where Δz is the length of the IFE base Cartesian cells in the z-direction. In the lateral directions, we use a uniform mesh size.

A typical numerical mesh used is also shown in Figure 6. In the simulations presented here, the upstream PIC and IFE mesh resolution is $\Delta z_{min} = h \simeq 5.25 \times 10^{-5}$m. This mesh size is less than the Debye length of the upstream discharging plasma and hence, it adequately resolves the upstream sheath. The PIC mesh size is $90 \times 52 \times 281$. The cartesian primary mesh used by IFE is $90 \times 52 \times 201$ (total number of finite element is 4,703,400). The number of streamlines tracked is typically about $117,000$ in each simulation loop.

C. The Cross-Over Limit

By varying the upstream plasma density, we can scan the operating envelope of an ion optics grid set and determine the cross-over and perveance limits. For each upstream density, we calculate the accel grid impingement current per hole J_a as well as the beamlet current J_b. Figure 7 shows the ratio of the impingement current of the accel grid to the beamlet current near cross-over, J_a/I_b, against J_b for several net accelerating voltage.

The J_a obtained from simulation includes only the contribution from beam ion impingement, $J_a = J_{imp}$. Hence, Figure 7 shows that J_a/J_b is zero over a wide range of upstream plasma density and becomes suddenly larger than zero when J_b becomes small. The cross-over limit in the simulation is defined as the location where J_a from becomes larger than zero. The cross-over limit obtained from simulation are compared with the that obtained from experiment in Figure 8. Figure 8 shows that both the experimental result and the numerical result have almost the same cross-over limit vs. accelerating voltage behavior. However, there is a constant difference between the experimental curve and the numerical curve. This is due to both the differences in the J_a/J_b values used to define the cross-over limit and the factors that are not included in the simulation, such as J_{cex} and $J_{leakage}$.

Since the charge-exchange current is proportional to the beam current, $J_{cex} \simeq CJ_b$, eq(1) can be rewritten as

$$\frac{J_a}{J_b} = \frac{J_{imp}}{J_b} + C + \frac{J_{leakage}}{J_b} \tag{7}$$

where C is a constant. The contributions from J_{cex} can be easily taken into account. However, the characteristics of $J_{leakage}$ is less clear.

In Figure 9, we compare the individual impingement current curve for several accelerating voltages. In addition to the experimental curve and the numerical curve, we also plot a "numerical-modified" curve, which is obtained by moving the the numerical curve to overlap with the experimental curve. Specifically, we move the origin of the coordinates used for plotting the numerical results from $(x, y) = (0, 0)$ to $(x, y) = (0.012, 4.5)$ in Figure 9. We find that the "numerical-modified" curves agree well with the experimental result.

The shift in the y coordinate (i.e. $\triangle \frac{J_a}{J_b} \simeq 4.5\%$) represents the contribution from J_{cex}. The results suggest that the contribution from the charge exchange ions to the accel current is $J_{cex} \simeq 0.045 J_b$. The shift in the x coordinate (i.e. $\triangle J_b \simeq 0.012$mA/hole) represents the effect from both $J_{leakage}$ and the differences in the definition of the cross-over limit. We are currently working on quantifying the experimental leakage currents as a function of operating condition and geometry.

D. Direct Impingement on Accel Grid

Figure 10 shows the potential and beamlet ion density contours for the $V_n = 1600$V and two upstream plasma conditions. The plots are for the $y = 0$ plane, which represents the horizontal plane cutting through the middle of the gridlet. At upstream density $n_0 = 0.05 \times 10^{17} m^{-3}$, the beamlet current just reached the cross-over limit.

We notice that the shape and size of the sheath changes drastically with the variation in the upstream density. More importantly, the beamlet through the edge aperture is asymmetrically focused more towards the gridlet center. As a result, the edge aperture of the accel grid experiences significant direct beam ion impingement on the portion oriented towards the center while the other parts of the accel grid sees no direct impingement. Figure 11 plots the distribution of beam ion impingement on the inside wall of three apertures

(the center aperture and two edge apertures) of the accel grid at cross-over. The results show that direct impingement is asymmetrically concentrated on the inboard portion of the aperture. This indicates that, when an ion optics operates near the cross-over limit, significant sputtering erosion would first occur to the edge apertures of the accel grid, and the erosion pattern on the edge apertures would be very asymmetrical.

IV. Summary and Conclusions

A coordinated experimental and modeling study is carried out to study ion impingement current limits. Sub-scale ion optics testing at CSU was completed on CBIO-like ion optics geometry over wide ranges of net and total accelerating voltage. Numerical simulations were carried out at VT to model a 7-aperture gridlet at cross-over using a new ion optics model. Very good agreement is observed between measurements and simulations of the cross-over limit. When the effects from the charge-exchange current and the leakage current are taken into account, modeling reproduces almost exactly the measured impingement current behavior. Simulations also show that the ion beamlets through circumferential apertures are focused more towards the optics center due to the asymmetry in electric field near the grid surface. Hence, when an ion optics operates near the cross-over condition, the edge apertures on the accel grid would experience significant direct ion impingement concentrated on the side oriented towards the optics center.

References

[1]Snyder, J. and Brophy, J., "Performance Characterization and Vibration Testing of 30-cm Carbon-Carbon Ion Optics," *40th AIAA/ASME/SAE/ASEE Joint Propulsion Conference and Exhibit*, AIAA 2004-3959, Ft. Lauderdale, FL, July 2004.

[2]Farnell, C., Williams, J., and Wilbur, P., "NEXT Ion Optics Simulation via ffx," *40th AIAA/ASME/SAE/ASEE Joint Propulsion Conference and Exhibit*, AIAA 04–4869, Fort Lauderdale, Florida, July 2004.

[3]Laufer, D. M., Williams, J. D., Farnell, C. C., Shoemaker, P. B., and Wilbur, P. J., "Experimental Evaluation of Sub-Scale CBIO Ion Optics Systems," *39th AIAA/ASME/SAE/ASEE Joint Propulsion Conference and Exhibit*, AIAA 03–5165, Huntsville, Alabama, July 2003.

[4]Kafafy, R. and Wang, J., "Whole Ion Optics Gridlet Simulations Using a Hybrid-Grid IFE-PIC Code," *Journal of Propulsion and Power*, 2006, accepted.

[5]Snyder, J., Brophy, J., and Anderson, J., "Results of a 1000-Hour Wear Test of 30-cm Carbon-Carbon Ion Optics," *41st AIAA/ASME/SAE/ASEE Joint Propulsion Conference and Exhibit*, AIAA 2005-4394, Tucson, AZ, July 2005.

[6]Kafafy, R. and Wang, J., "A Hybrid–Grid Immersed–Finite–Element Particle–in–Cell Algorithm for Modeling Spacecraft Plasma Interactions," *IEEE Transactions on Plasma Science*, 2006, accepted.

[7]Wang, J., Cao, Y., Kafafy, R., Pierru, J., and Decyk, V., "Ion Propulsion Plume Simulations Using Parallel Supercomputer," *IEEE Transactions on Plasma Science*, 2006, accepted.

[8]Kafafy, R., Lin, T., Lin, Y., and Wang, J., "Three Dimensional Immersed Finite Element Methods For Electric Field Simulation In Composite Materials," *International Journal for Numerical Methods in Engineering*, Vol. 64, August 2005, pp. 940–972.

[9]Wang, J., Polk, J., Brophy, J., and Katz, I., "Three-Dimensional Particle Simulations of Ion-Optics Plasma Flow and Grid Erosion," *Journal of Propulsion and Power*, Vol. 19, No. 6, 2003, pp. 1192–1199.

Figure 1: High voltage sub-scale ion optics testing facitility

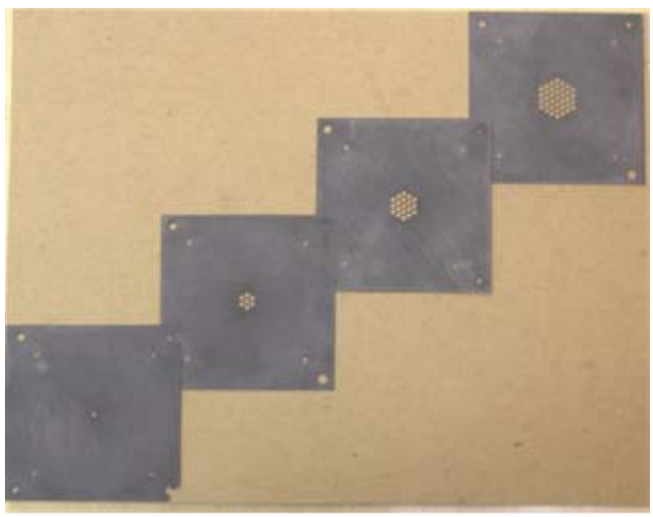

Figure 2: Sub-scale CBIO-style Poco graphite grids.

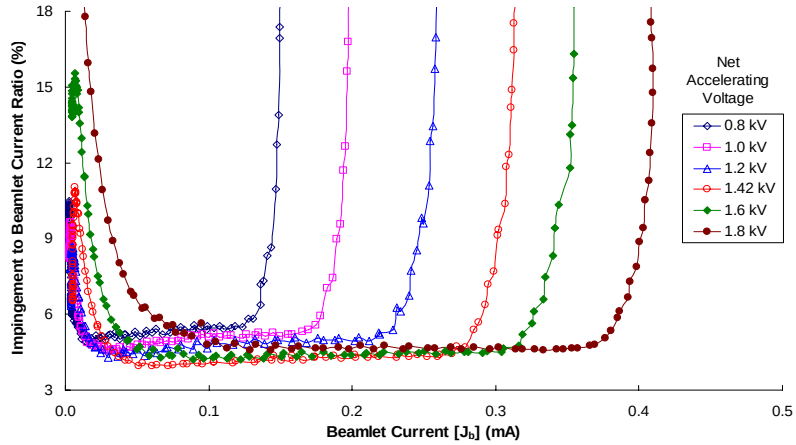

Figure 3: Experimental Results: Impingement current behavior for 7-hole gridlet

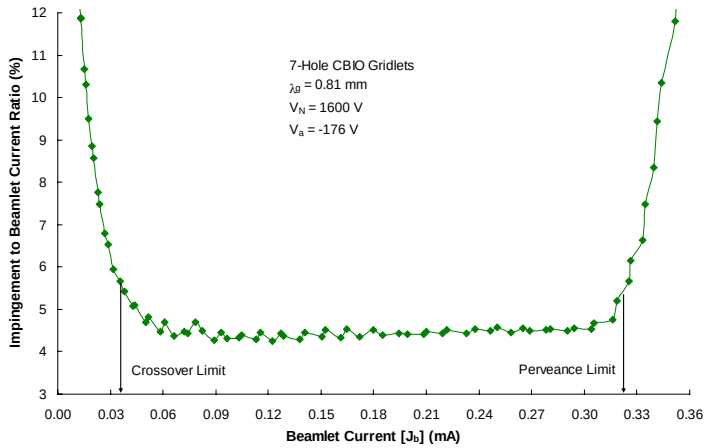

Figure 4: Experimental Results: Impingement current behavior for 7-hole gridlet operated at V_N=1600V, with cross-over limit and preveance limit definitions.

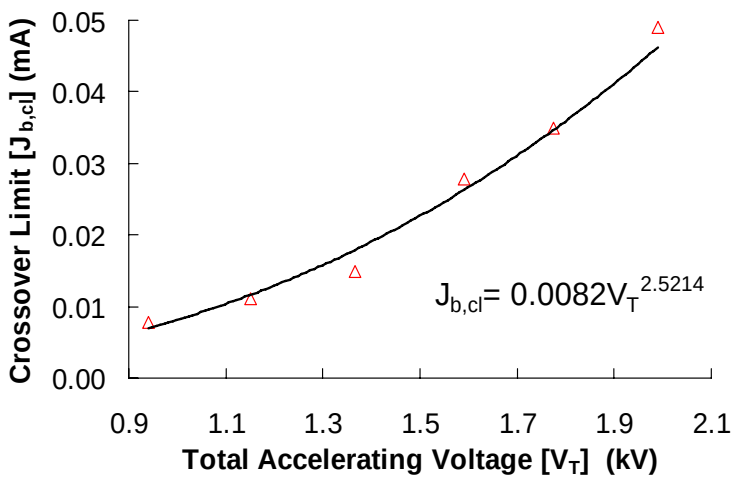

Figure 5: Experimental Results: Cross-over behavior for 7-hole gridlet vs. total accelerating voltage

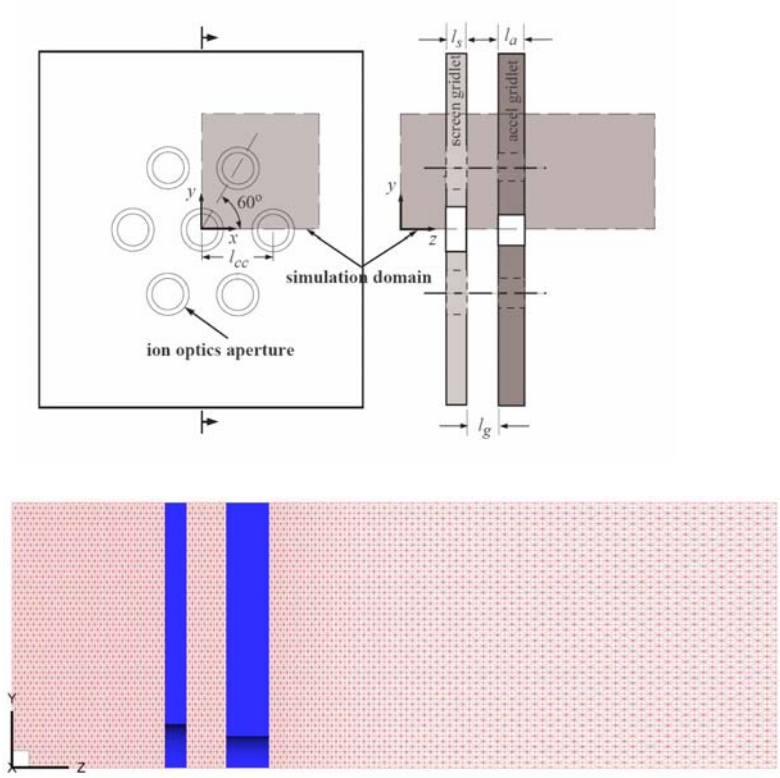

Figure 6. Simulation setup and typical simulation mesh.

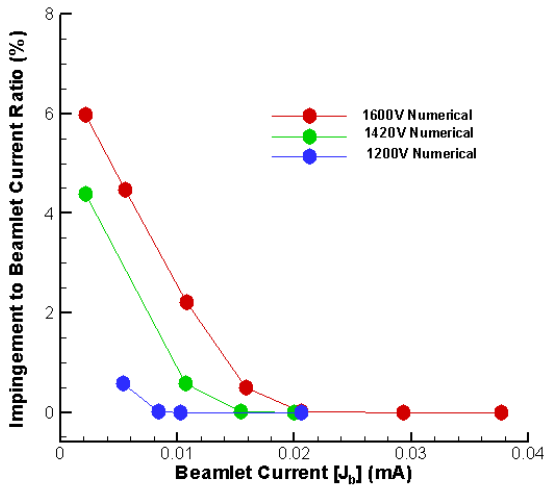

Figure 7: Simulation Results: Impingement current behavior for 7-hole gridlet at cross-over

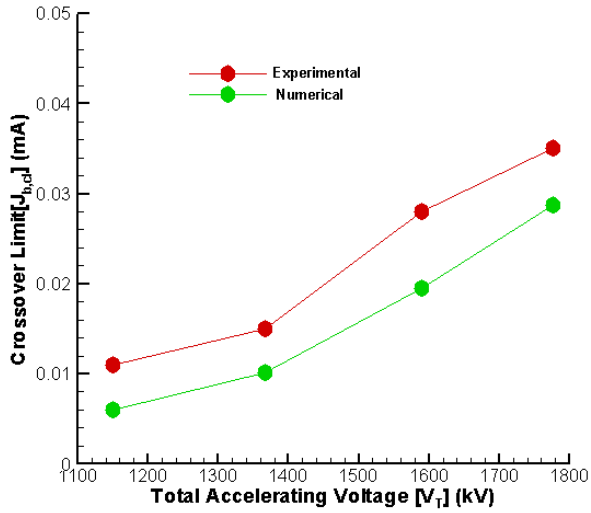

Figure 8. Comparison of Simulations with Measurements: Cross-over behavior for 7-hole gridlet vs. net accelerating voltage.

a) 1200V

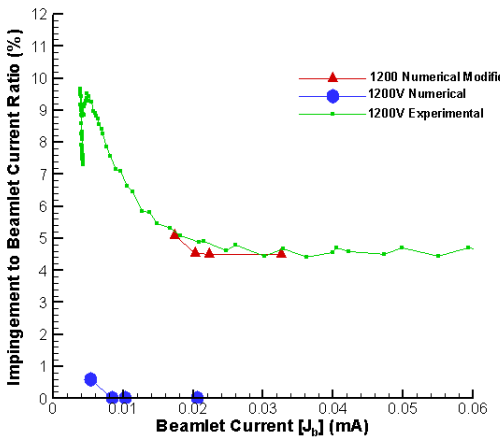

b) 1420V

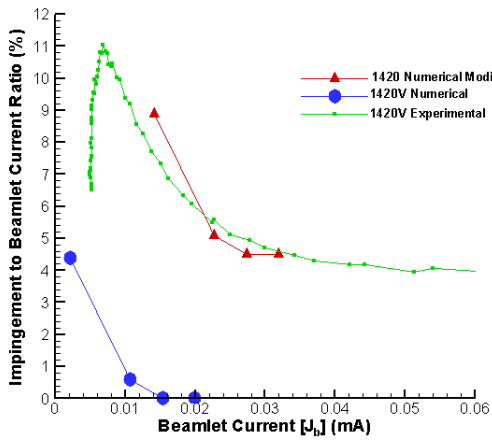

c) 1600V

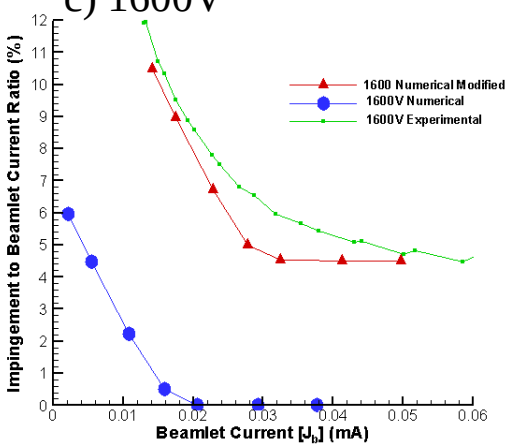

Figure 9: Comparison of Simulations with Measurements: Impingement current behavior for 7-hole gridlet at cross-over. The “numerical-modified” lines are obtained by shifting the “origin” of the coordinates used for plotting the simulation results from (x,y)=(0,0) to (x,y)=(0.012, 4.5).

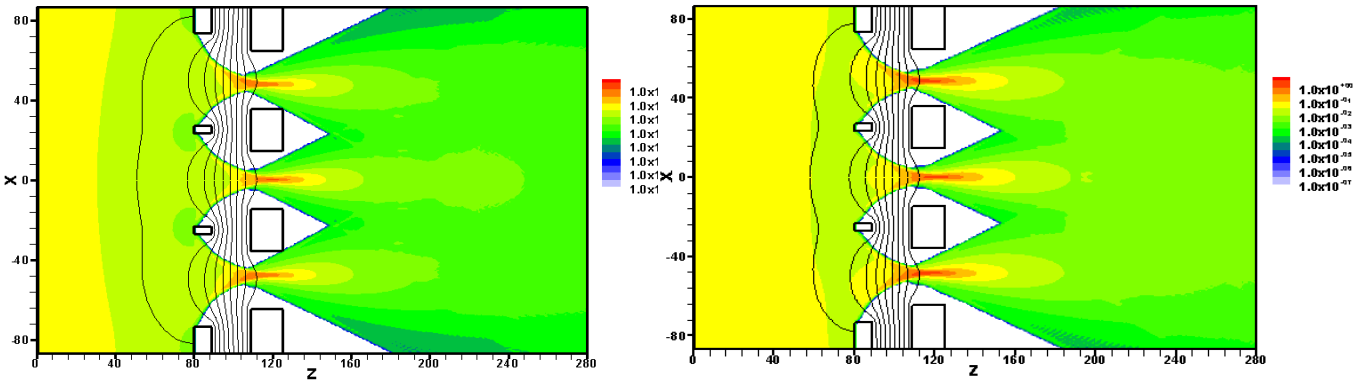

a) n_0=0.05E17m^{-3}, J_b=0.01082mA

b) n_0=0.1E17m^{-3}, J_b=0.02054mA

Figure 10: Simulation Results: Beamlet potential and ion density (V_N=1600V). The unit for on density contour level is 1E17m^{-3}. The interval in potential contours levels is 200V.

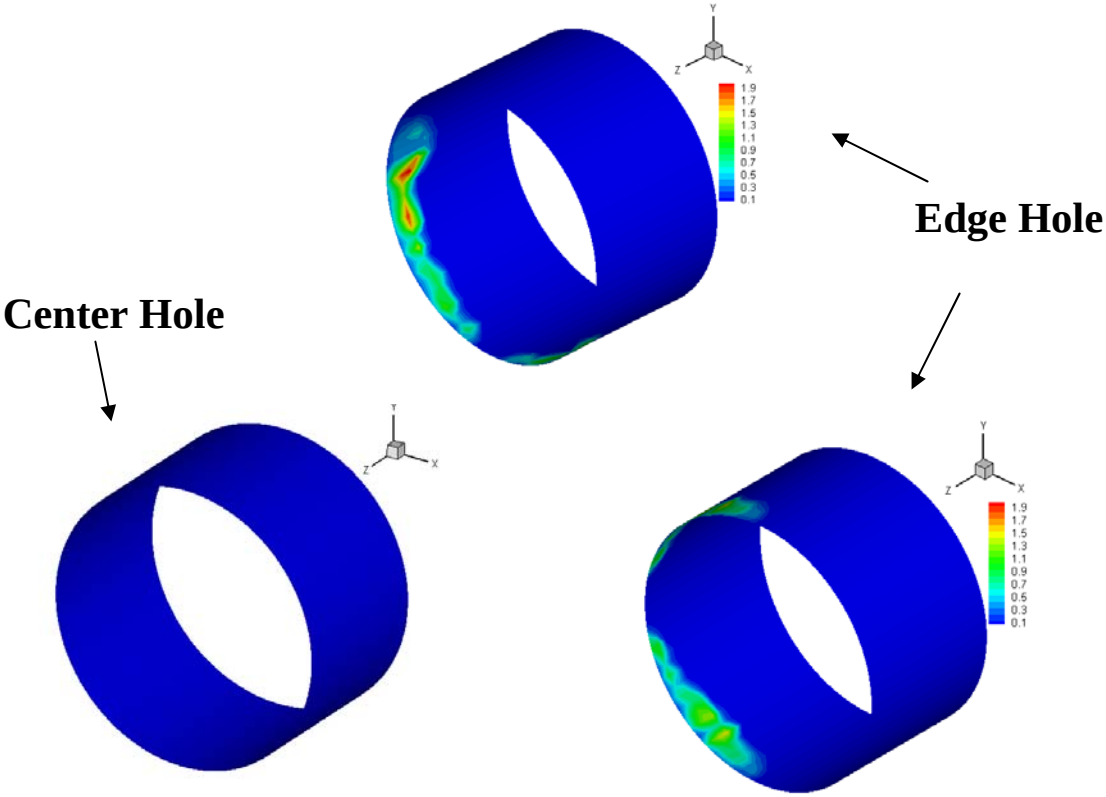

Figure 11: Simulation Results: Beam ion impingement current density distribution on the accel grid aperture wall at cross-over (n_0=0.05E17m^{-3}, V_N=1600V). The view angle is from the down stream side of the accel gird (contour level unit: mA/mm^2).